Shock Waves (2002) 1: 271–278

Shock Waves
© Springer Verlag 2002

Effect of boundary layer on Mach reflection over a wedge surface

T. Adachi[1], A. Sakurai[2], S. Kobayashi[1]

[1] Department of Mechanical Engineering, Saitama Institute of Technology, Saitama 369–0293, Japan
[2] Department of Mathematical Sciences, Tokyo Denki University, Tokyo 101–0054, Japan

Received 6 March 2000 / Accepted 23 April 2001

Abstract. In this paper, we consider the phenomenon of unsteady Mach reflection generated by a plane shock wave advancing over a straight wedge surface, with particular attention to the deviation of the flow field from the self-similar nature. We examine the observed change in angle between incident and reflected shocks, which is in contrast to the fact that the angle should remain constant with time in a self-similar flow. The effect of the boundary layer behind the advancing shock wave over the surface of the wedge is considered to cause this, and boundary layer theory is utilized to estimate the thickness of the layer. It is found that the thickness increases as $\sqrt{t}$ to the time t compared with t by the overall expansion in the self-similar flow. Assuming that the thicker boundary layer is effectively equivalent to a change in wedge angle, the effect of the boundary layer on the flow field should be less in later stages with larger t values in accordance with the observation above.

Key words: Mach reflection, Non self-similar nature, Boundary layer

1 Introduction

We consider the phenomenon of unsteady Mach reflection generated by a plane shock wave advancing over a straight wedge surface. Although the overall features of the phenomenon can be seen from past experiments as well as numerical simulation, there have been some renewed interest in its crucial details, especially for its weak cases (Itabashi et al. 1997; Kobayashi et al. 1997; Henderson et al. 1997). These are mostly concerned with observing various deviations of the flow field from the self-similar nature. A close look at Fig. 1, which is for the development of the reflection of a plane shock wave advancing over a straight wedge, and the trajectory of its triple point shown in Fig. 2, both of which are seen to exhibit a self-similar nature of the phenomenon, reveals the deviation as explained below.

Here we are interested in the change in the angle ω_{ir} between incident i and reflected r shocks (Kobayashi et al. 1997) as seen in Figs. 3 and 4. Since an angle in a self-similar flow should remain constant with time, the above clearly indicates at least a temporary deviation before the change settles down to null as is seen in Fig. 4, where we can see the deviation from the constant state being emphasized in lower Mach number case as it should be expected for viscous effects. The self-similar nature of the flow field is based on the fact that there is no proper influential length scale to the flow field and the length scale due to the viscosity is usually not so influential. However, this scale can be effective in some critical cases, especially

Correspondence to: T. Adachi (e-mail: adachi@sit.ac.jp)

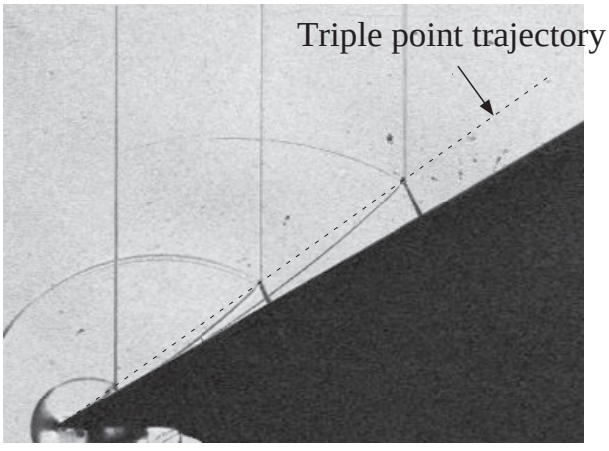

Fig. 1. Development of reflection ($M_i = 1.40$, $\theta_w = 30.20°$)

that of weak Mach reflection where its three-shock pattern is known to be sensitive to the configuration of the flow field (Sakurai 1964). In fact, this kind of change is not observed in a boundary-layer-free experiment in the reflection of two shock waves (Skews 1989). The purpose of this present paper is to correlate the change with the behavior of the boundary layer generated by the advancing Mach stem over the flat surface.

2 Effects of viscosity on self-similar flow

The effects of viscosity on Mach reflection phenomenon have previously been discussed in general [for example,

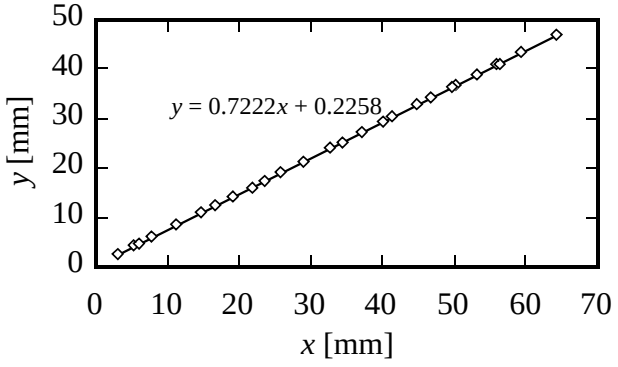

Fig. 2. Triple point trajectory. The x-axis is taken along the wedge surface and the y-axis is perpendicular to it. The incident shock Mach number M_i is 1.40 and the wedge angle θ_w is 30.20°

(Hornung 1986; Sakurai et al. 1989; Henderson et al. 1997)], and we consider the problem with the Navier-Stokes equation expressed in self-similar variables. Let (x, y) be a coordinate system with its origin O for the apex of the wedge as in Fig. 5; $\mathbf{v} = (u, v)$, the velocity; p, the pressure; ρ, the density; T, the temperature of the flow field; and t, time starting when the incident shock wave arrives at the apex of the wedge. The Navier-Stokes equations of continuity, momentum and energy for a two-dimensional, viscous, heat conducting, ideal gas flow are given as

$$\frac{D\rho}{Dt} + \rho\, div\, \mathbf{v} = 0$$

$$\rho\frac{D\mathbf{v}}{Dt} = -grad\, p + \frac{\mu}{3}\, grad\, div\, \mathbf{v} + \mu\Delta\mathbf{v} \qquad (1)$$

$$\frac{p}{\gamma - 1}\frac{D}{Dt}[\log(p\rho^{-\gamma})] = \mu\left[2\left\{\left(\frac{\partial u}{\partial x}\right)^2 + \left(\frac{\partial v}{\partial y}\right)^2\right\} + \left(\frac{\partial u}{\partial y} + \frac{\partial v}{\partial x}\right)^2 - \frac{2}{3}(div\ \mathbf{v})^2\right] + \kappa\Delta T$$

where κ and μ are the coefficients of heat conduction and viscosity, respectively.

We now introduce the dimensionless similarity variables X, Y, U, V, P and R defined by

$$X = \frac{x}{ct},\ Y = \frac{y}{ct},\ U = \frac{u}{c} - X,\ V = \frac{v}{c} - Y,$$

$$P = \frac{p}{p_1},\ R = \frac{\rho}{\rho_1} \qquad (2)$$

and use

$$s = \frac{\mu}{\gamma p_1 t}$$

where γ is the ratio of specific heats, p_1 and ρ_1 are the pressure and the density values of a certain uniform state, and

$$c^2 = \gamma p_1/\rho_1.$$

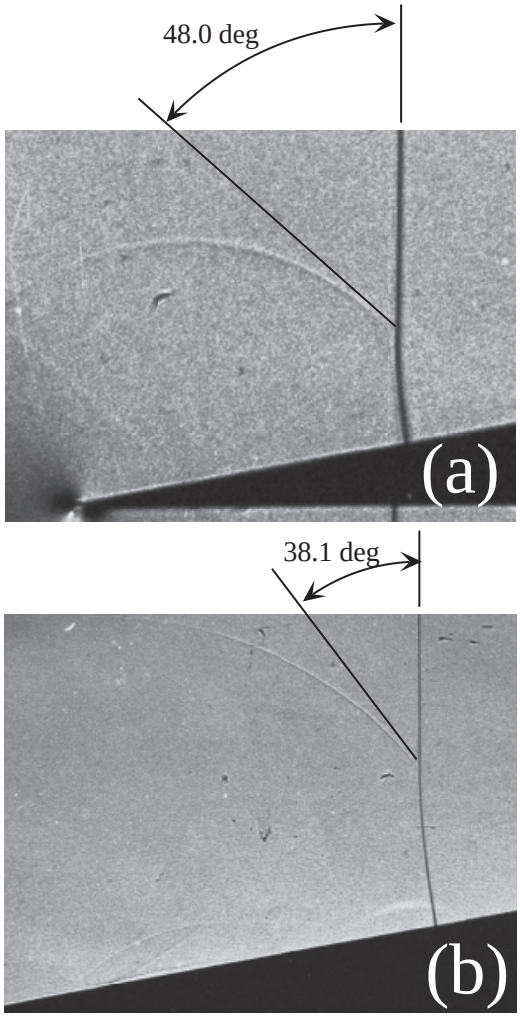

Fig. 3a,b. Visualization of the decrease in ω_{ir} for $M_i = 1.30$ and $\theta_w = 10.75°$. **a** $x = 14.87$ mm. **b** $x = 55.52$ mm

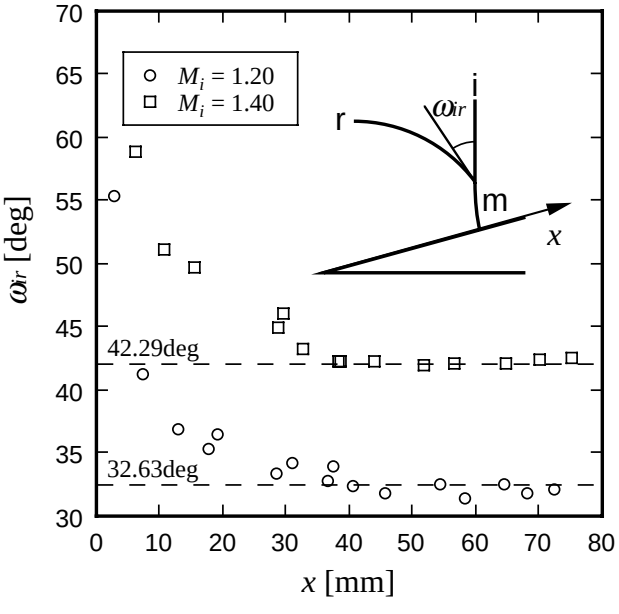

Fig. 4. Variation of ω_{ir} ($\theta_w = 15°$)

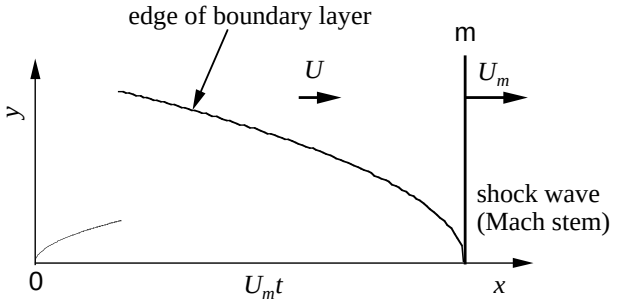

Fig. 5. Boundary layer over the wedge surface

We then have the relations

$$\frac{D}{Dt} = \frac{1}{t}\left[U\frac{\partial}{\partial X} + V\frac{\partial}{\partial Y} - s\frac{\partial}{\partial s}\right],$$

$$div\,\mathbf{v} = \frac{1}{t}[U_X + V_Y + 2],$$

$$\begin{aligned}\frac{p}{\gamma-1}\frac{D}{Dt}[\log(p\rho^{-\gamma})] &= \frac{1}{\gamma-1}\left[\frac{Dp}{Dt} - \gamma\frac{p}{\rho}\frac{D\rho}{Dt}\right]\\ &= \frac{1}{\gamma-1}\left[\frac{Dp}{Dt} + \gamma p\,div\,\mathbf{v}\right]\\ &= \frac{p_1}{t(\gamma-1)}[UP_X + VP_Y - sP_s\\ &\quad +\gamma P(U_X + V_Y + 2)],\end{aligned}$$

$$\begin{aligned}\kappa\Delta T &= \frac{\kappa}{c^2t^2}[T_{XX} + T_{YY}]\\ &= \frac{1}{\sigma}\frac{\mu}{t^2(\gamma-1)}\left[\left(\frac{P}{R}\right)_{XX} + \left(\frac{P}{R}\right)_{YY}\right],\end{aligned}$$

assuming an ideal gas and the Prandtl number σ.

The system of Eq. (1) is transformed into

$$UR_X + VR_Y + R(U_X + V_Y + 2) = sR_s,$$

$$\begin{aligned}&R(UU_X + VU_Y + U) + \frac{1}{\gamma}P_X\\ &\quad = s\left[RU_s + \frac{1}{3}(U_X + V_Y)_X + U_{XX} + U_{YY}\right]\end{aligned}$$

$$\begin{aligned}&R(UV_X + VV_Y + V) + \frac{1}{\gamma}P_Y\\ &\quad = s\left[RV_s + \frac{1}{3}(U_X + V_Y)_Y + V_{XX} + V_{YY}\right] \qquad (3)\end{aligned}$$

$$\begin{aligned}&UP_X + VP_Y + \gamma P(U_X + V_Y + 2)\\ &\quad = s\left[P_s + (\gamma-1)\left\{2(U_X+1)^2 + 2(V_Y+1)^2\right.\right.\\ &\qquad +(U_Y + V_X)^2 - \frac{2}{3}(U_X + V_Y + 2)^2\Big\}\\ &\qquad +\frac{\gamma}{\sigma}\left\{\left(\frac{P}{R}\right)_{XX} + \left(\frac{P}{R}\right)_{YY}\right\}\Big]\end{aligned}$$

(see Sakurai et al. 1989).

While the left-hand sides of Eq. (3) altogether represent the non-viscous, self-similar flow field, the effect of viscosity (and heat conductivity as well) on the field, is given by the the right-hand sides of Eq. (3). Each of these terms is seen to be multiplied by the variable s $(=\mu/\gamma p_1 t)$, which is negligibly small in a usual situation so that we may expect to have self-similar flow in general. However, these terms can be significant in some cases. For example, the early stage of $t \approx 0$ should have large s values, and indeed this can be the cause for the RR $\rightarrow$ MR transition there [Fig. 6 (Itabashi et al. 1997; Walenta 1987; Henderson et al. 1997)] as well as the bent triple point trajectory that is supposed to be a straight line through the apex of the wedge to the self-similar flow [Fig. 7 (Walenta 1987)]. Still another significant effect is expected from higher derivatives appearing in the right-hand sides of Eq. (3), which can become large enough near the surface to effectively surpass small factor s. We will examine the effect of this boundary layer and correlate this with the flow behind the advancing Mach wave.

3 Effect of boundary layer over the wedge surface

Consider the boundary layer generated by the advancing Mach stem m (shock wave) over a wedge surface (Fig. 5). Another boundary layer starts from the apex of the wedge and may possibly be combined with or embedded in the first layer as illustrated in the figure. There is also the problem of the thermal boundary layer that interacts with the above layer through the compressibility of the fluid. Here we assume for the sake of simplicity that the main flow is uniform and the flow in the boundary layer is incompressible. We can thus examine the effect of the former boundary layer in a separate way from the latter and thermal one. Take $y = 0$ for the surface of the wedge and let U be the main flow velocity behind the Mach stem m propagating with velocity U_m (Fig. 5). Previous papers have investigated on the boundary layer generated by an advancing shock wave over a plate (Hornung 1986; Becker 1961; Mirels 1958; Schlichting 1979). They indicate the growth of thickness of the layer with time. Here we construct an approximate solution so that we can see the growth explicitly.

The equation of momentum conservation in the boundary layer is given for the velocity u as

$$U\frac{\partial\delta}{\partial t} + U^2\frac{\partial\delta_M}{\partial x} = \nu\left(\frac{\partial u}{\partial y}\right)_{y=0}, \quad U = \text{constant} \qquad (4)$$

where δ and δ_M are the displacement and momentum thickness and are given respectively as

$$\delta = \int_0^\infty \left(1 - \frac{u}{U}\right)dy, \quad \delta_M = \int_0^\infty \frac{u}{U}\left(1 - \frac{u}{U}\right)dy \qquad (5)$$

so that

$$\delta(U_m t, t) = 0 \qquad (6)$$

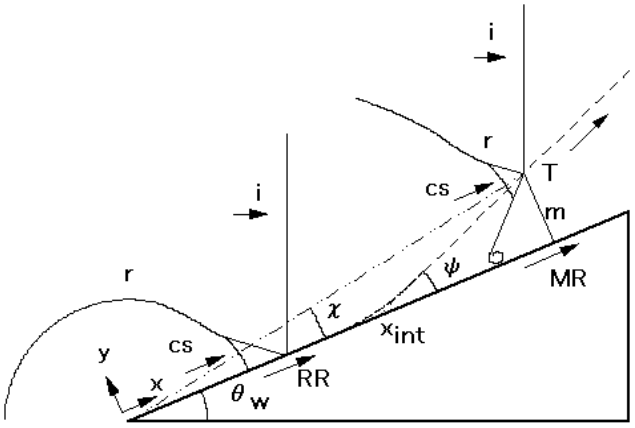

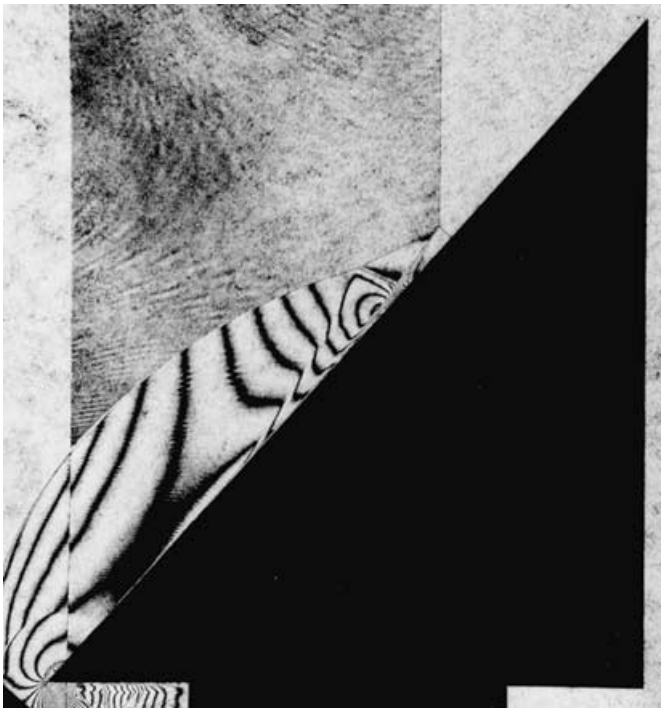

Fig. 6. Schematic of the RR→MR transition on the ramp and double exposure holographic interferogram [(Itabashi et al. 1997) $M_i = 2.332$, $\theta_w = 52°$]

and ν is the coefficient of kinematic viscosity.

We utilize the Kármán-Pohlhausen approximation (unsteady)

$$u = \begin{cases} U \sum_{i=1}^{4} C_i(x,t)(\frac{y}{\delta})^i, & 0 \le y \le \delta \\ 0, & y > \delta \end{cases}$$

with the boundary conditions

$$y = 0: \quad u = \frac{\partial^2 u}{\partial y^2} = 0,$$

$$y = \delta: \quad u = U, \quad \frac{\partial u}{\partial y} = \frac{\partial^2 u}{\partial y^2} = 0$$

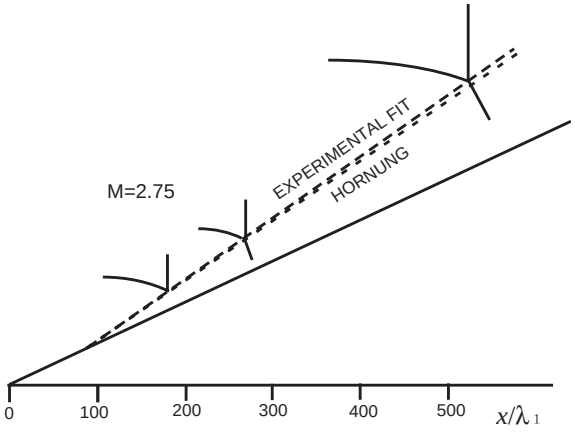

Fig. 7. Low density gas experiment (Walenta 1987)

to yield

$$\frac{\partial \delta^2}{\partial t} + a\frac{\partial \delta^2}{\partial x} = b, \quad a = \frac{74}{189}U, \quad b = \frac{40\nu}{3}$$

which is integrated to

$$\delta^2 = \frac{b}{2}\eta \; + \; f(\xi), \quad \xi = t - \frac{x}{a}, \quad \eta = t + \frac{x}{a}$$

with $f(\xi)$ being an arbitrary function to be determined by condition (6). Finally, we have

$$\delta = \sqrt{\frac{b}{U_m - a}}\sqrt{U_m t - x}\,. \tag{7}$$

Equation (7) shows that the thickness grows with the time t as $\sqrt{t}$, as we can see from

$$\delta(0,t) = A\sqrt{\nu t}, \quad A^2 = \frac{7860}{382 + 185M^{-2}}$$

where M is the Mach number of the Mach stem. The boundary layer thickness behind the Mach stem is shown in Fig. 8 with the present experimental conditions in Fig. 1. However, the global flow field expands as t in the self-similar flow, so that the thickness decreases as $1/\sqrt{t}$ relative to the main flow. The situation is expressed better in the self-similar variables as

$$\bar{\delta} \equiv \frac{\delta(x,t)}{U_m t} = \frac{A}{\sqrt{\gamma}}\frac{\sqrt{s}}{M}\sqrt{1 - \frac{x}{x_m}}$$

and it is shown schematically in Fig. 9, where $\bar{\delta}$ indeed decreases as $1/\sqrt{t}$.

4 Concluding remarks

If we accept that the thicker boundary layer is effectively equivalent to the change in wedge angle, the effect of the boundary layer on the flow field should be large in the beginning and become less in later stages with increasing time t; this is in accordance with the observations in Figs. 3

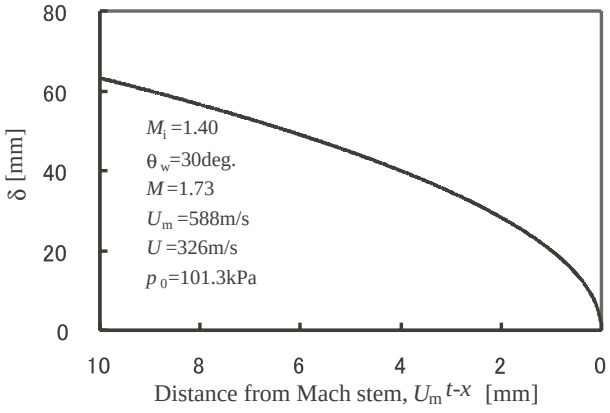

Fig. 8. Boundary layer thickness behind the Mach stem calculated by Eq. (7) with the experimental conditions of Fig. 1

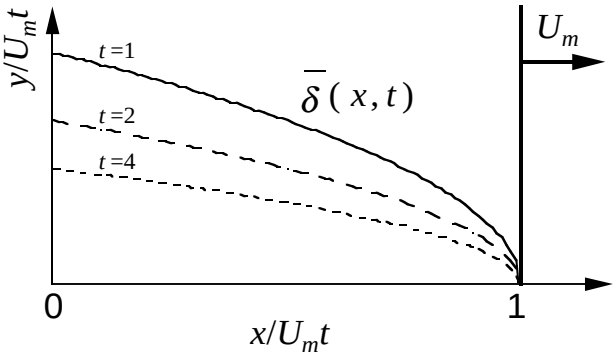

Fig. 9. Decrease of boundary layer thickness with increasing time in self-similar variables

and 4. In examining this in more detail, we first notice the ω_{ir} values settling to a certain level after decreasing with time; shown as 38.1° for $M_i = 1.30$ in Fig. 3, about 32° for $M_i = 1.20$ and 42° for $M_i = 1.40$ in Fig. 4. They should be correlated with the corresponding values given by the self-similar solution expressed in an explicit form for weak cases as (Kobayashi et al. 1997)

$$\omega_{ir} = \cos^{-1}\sqrt{\frac{M_i^2+5}{7M_i^2-1}} \qquad (\gamma = 1.4)\ .$$

Indeed, this gives, $\omega_{ir} = 32.63°, 38.19°$ and 42.29° for $M_i = 1.2$, 1.3 and 1.4, respectively, which compares well with the above values.

Next, we see how the thin boundary layer can change ω_{ir} from the self-similar value above. In fact, the actual boundary layer is estimated to be very thin, on the order of several tens of microns, based on Eq. (7) in the present experimental set-up as shown in Fig. 8. It should be noted in this regard that the three-shock configuration is known to be sensitive to the change of the wedge angle, especially for weak cases, as can be found in Appendix A (Sakurai 1964).

Let us consider the feature in the following somewhat simplified situation. The configuration of the three-shock system for Mach reflection can be given by the three-shock theory, where we have two equations, Eq. (A4) or

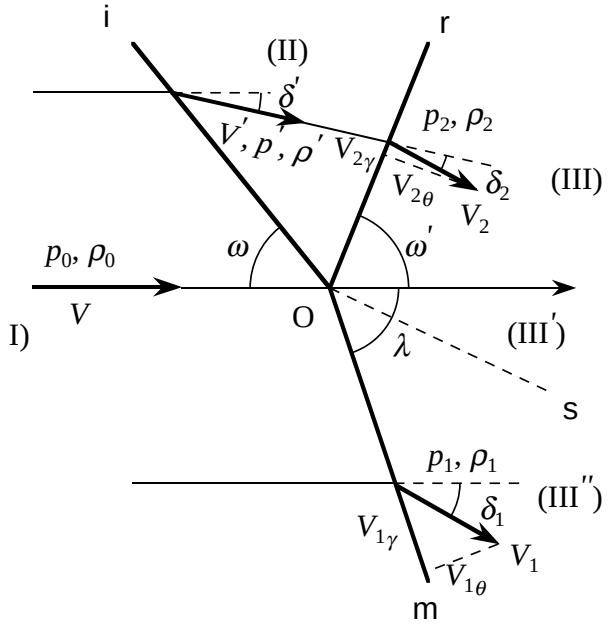

Fig. 10. Flow field of the stationary Mach reflection in the coordinate attached to the triple point

Eqs. (A5) and (A6), to determine two unknowns, ω' and λ, for given ϵ and ω in Eq. (A1). This procedure can be very sensitive to a small change in M or ω, especially for weak cases. The reason for this is due to the fact that terms including ω' in these equations become very small in the case, as we can see in Table 1 in Appendix A where they are as small as $10^{-4} \sim 10^{-7}$.

We consider this in a more explicit way in Appendix B to a modified three-shock condition (B1), where the effect of viscous layers is added to the original condition (A4) through the terms a, b to represent the small change above. The real situation is more involved, but, in any case, the essential feature can be as such to give a change in ω' from a change in ω caused by the boundary layer thickness, so that the expected boundary layer can be sufficiently thin to significantly change the pattern.

Appendix A

Consider the flow field of a stationary Mach reflection [Fig. 10 (Sakurai 1964)] consisting of three steady shock waves, incident i, reflected r and Mach wave m, and a slip line s. It is assumed that the flow field in region (I) is uniform and the shock wave i is a plane shock wave. The flow field in region (II) is also uniform. Region (III) is bounded by two shock waves, r and m, and includes a slip line s, dividing the region into two uniform subregions (III′) and (III″). Assuming V, p_0, and ρ_0 as the velocity, pressure, and density of the uniform flow region (I), then the velocity V', its deflection angle δ' from the velocity in (I), the pressure p' and the density ρ' in the uniform region (II) are given by the shock condition at the shock wave i, and we have

$$\frac{p'}{p_0} \equiv \frac{1}{\xi} = 1 + \frac{2\gamma}{\gamma+1}\epsilon, \quad \epsilon = M^2\sin^2\omega - 1, \qquad \text{(A1)}$$

$$\tan\delta' = \epsilon\left(\frac{\gamma+1}{2}M^2-\epsilon\right)^{-1}\cot\omega,$$

where ω is the incident shock angle defined by the angle between i and V as shown in Fig. 10, M is the Mach number of the incident wave i, and γ is the ratio of specific heats.

Let us call the angles between the flow direction of V and r, ω', and that of V and m, λ, respectively (cf. Fig. 10). Pressure p_1 and deflection angle δ_1 at the shock wave m are then given as

$$\frac{p_1}{p_0} = 1+\frac{2\gamma}{\gamma+1}\epsilon_1, \quad \epsilon_1 = M^2\sin^2\lambda - 1, \tag{A2}$$

$$\tan\delta_1 = \epsilon_1\left(\frac{\gamma+1}{2}M^2-\epsilon\right)^{-1}\cot\lambda.$$

Similarly, the corresponding quantities p_2 and δ_2 at the shock wave r are given by

$$\frac{p_2}{p_0} = \frac{p_2}{p'}\frac{p'}{p_0} = \left(1+\frac{2\gamma}{\gamma+1}\epsilon_2\right)\left(1+\frac{2\gamma}{\gamma+1}\epsilon\right),$$

$$\epsilon_2 = M'^2\sin^2(\omega'+\delta') - 1, \tag{A3}$$

$$\tan\delta_2 = -\epsilon_2\left(\frac{\gamma+1}{2}M'^2-\epsilon_2\right)^{-1}\cot(\omega'+\delta'),$$

where M' is the Mach number of the flow in (II).

The problem of stationary Mach reflection is to determine its configuration represented by the angles ω' and λ, which depend on the configuration of the incident shock wave produced by its angle ω and strength ϵ (or ξ). For this purpose, the three-shock theory utilizes the continuity in the pressure as well as in the flow direction across the line s. This leads to the following conditions:

$$\Delta p = p_2 - p_1 = 0, \quad \Delta\delta = \delta' + \delta_2 - \delta_1 = 0. \tag{A4}$$

Let us write conditions (A4) in more detail using Eqs. (A1), (A2) and (A3) as

$$\epsilon_2 + \epsilon - \epsilon_1 + \frac{2\gamma}{\gamma+1}\epsilon\epsilon_2 = 0, \tag{A5}$$

$$\tan^{-1}\left[\epsilon\left(\frac{\gamma+1}{2}M^2-\epsilon\right)^{-1}\cot\omega\right] + \tan^{-1}\left[-\epsilon_2\left(\frac{\gamma+1}{2}M'^2-\epsilon_2\right)^{-1}\cot(\omega'+\delta')\right] - \tan^{-1}\left[\epsilon_1\left(\frac{\gamma+1}{2}M^2-\epsilon_1\right)^{-1}\cot\lambda\right] = 0. \tag{A6}$$

It will now be shown that the terms in Eqs. (A5) and (A6), including ω' appear to be very small for the observed ω' values of weak shock experiments, which always give values very close to 90 degrees. Variable ϵ_2 is expressed as

$$\epsilon_2 = M'^2 - 1 - M'^2\cos^2(\omega'+\delta')$$

and ω' occurs in fact in Eq. (A6) through $\cos^2(\omega'+\delta')$. Since δ' turns out to be a small, positive angle in these cases, the angles $\omega'+\delta'$ become almost 90 degrees for the experimental ω' values and $\cos^2(\omega'+\delta')$ values are very small for these values. As for the second term in Eq. (A6), we have a factor $\cot(\omega'+\delta')$, which is small, and another small factor, ϵ_2, which also becomes small for the weak case, since M' is very near to 1 in this case. Let us check these in more detail numerically by taking $\xi = 0.9$ ($\epsilon = 2/21$) and using the measured values of ω' such as given in the references (Harrison and Bleakney 1947). The results are tabulated in Table 1, where we can see that the terms are indeed very small. This suggests the sensitivity of the systems to the amount of ω', so that a small change in the configuration of the incident shock wave can cause a significant change in the amount of ω'.

Appendix B

Consider the modified three-shock condition (Adachi et al. 1992),

$$\Delta p = a, \quad \Delta\delta = b \tag{B1}$$

where a and b are the terms representing the effect of viscous layers for the differences in pressure and shock angle, respectively. The feature of the solution of (B1) was studied numerically for a, b values given parametrically a priori (Adachi et al. 1992). It was found that the case of $a = 0$, $b \neq 0$ agreed well with corresponding experimental data in comparison with the case of $a \neq 0$, indicating that the pressure difference is negligible as it should be in a viscous layer. Results of (ω, ω') values for $M_i = 1.41$ ($\epsilon = 0.98$) with $a = 0$ and various b values are shown graphically in Fig. 11 We can notice in the figure that branches of (ω, ω')-curves for various $b(\neq 0,$ small values) near MR(trivial) curve of $b = 0$ are almost perpendicular to the ω-axis in the crucial area near $\omega \approx 60°$, indicating that a small change in b or the existence of a small non-zero b itself can result in a significant change in ω'. In the followings, we will see this in a more specific way in an appropriate expression of the solution of (B1). We have from (B1) with $a = 0$ with use of (A1), (A2) and (A3) that

$$\epsilon_2 \cdot B(\epsilon,\omega;\epsilon_2,\lambda) = \tan b \equiv b' \tag{B2}$$

where B is given as

$$B = \left[-\frac{\cot(\omega'+\delta')}{\frac{\gamma+1}{2}M'^2-\epsilon_2} + \frac{1+\frac{2\gamma}{\gamma+1}\epsilon}{1+A'A_1}\cdot\frac{A_1}{\sin\lambda\ \cos\lambda} \times\left\{-\frac{\gamma+1}{2}\frac{1+\epsilon_1}{\epsilon\epsilon_1}A' + \frac{1}{1+\epsilon}\cdot\frac{1}{(\cot\omega+\cot\lambda)}\right\}\right] \times\left(1+A_2\frac{A'-A_1}{1+A'A_1}\right)^{-1} \tag{B3}$$

$$A' = \tan\delta = \frac{\sin\omega\ \cos\omega\ \cdot\epsilon}{\frac{\gamma+1}{2}(1+\epsilon)-\epsilon\sin^2\omega},$$

$$A_1 = \tan\delta_1 = \frac{\sin\lambda\cos\lambda\cdot\epsilon_1}{\frac{\gamma+1}{2}(1+\epsilon_1)-\epsilon_1\sin^2\lambda},$$

Table 1. $\cos^2(\omega'+\delta')$, $\epsilon_2\{(\gamma+1)/2\cdot M'^2-\epsilon_2\}^{-1}\cot(\omega'+\delta')$ values derived from experimental ω' values

ω	68.0	71.6	73.6	65.6	66.6	67.2	73.5	72.0	73.9°
ω'	86.9	88.3	89.1	84.2	85.7	86.4	88.9	87.9	88.2°
δ'	1.5	1.3	1.2	1.7	1.6	1.6	1.2	1.3	1.2°
$\cos^2(\omega'+\delta')\times 10^4$	8	0.1	0.001	60	20	10	0.01	0.1	0.1
$\epsilon_2\{(\gamma+1)/2\cdot M'^2-\epsilon_2\}^{-1}$	6	0.01	−0.02	5	2	1	−0.0002	0.04	0.02
$\times\cot(\omega'+\delta')\times 10^4$									

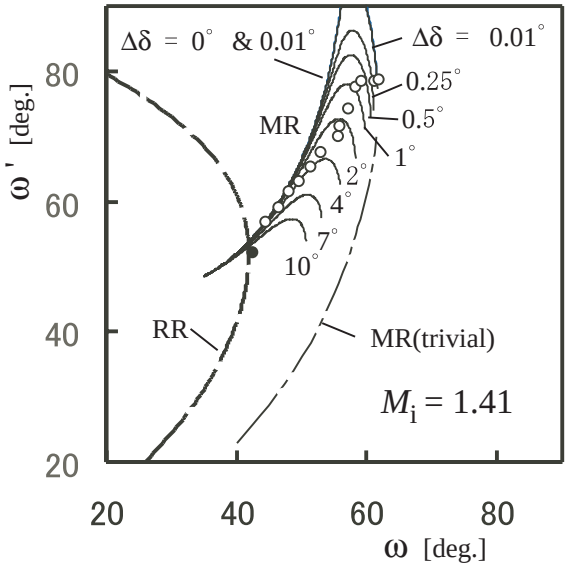

Fig. 11. Relation between angles of incidence and reflection. $M_i = 1.41$. Open and solid circles denote experimenatal data for Mach and regular reflections, respectively. Solid line, dashed line and dash-dotted line denote modified three-shock, two-shock and trivial solutions, respectively

$$A_2 = \tan\delta_2 = \frac{-\cot(\omega'+\delta')\cdot\epsilon_2}{\frac{\gamma+1}{2}M'^2-\epsilon_2}\ ,$$

$$\frac{1+\epsilon_1}{1+\epsilon} = \frac{\sin^2\lambda}{\sin^2\omega}\ , \qquad \epsilon_2 = M'^2\sin^2(\omega'+\delta')-1$$

$$M'^2 = \left[2+\frac{(\gamma-1)(1+\epsilon)}{\sin^2\omega}\right] \times\left[\frac{1}{\gamma+1+2\gamma\epsilon}+\frac{2}{\gamma-1}\cdot\frac{1}{\gamma+1+(\gamma-1)\epsilon}\right]-\frac{2}{\gamma-1}\,.$$

We have $\epsilon_2\cdot B\equiv b'$ (B2), and consider first the case of $b'=0$ or the original three-shock condition (A4), to which we have either (i) $\epsilon_2=0$ or (ii)$B=0$. The first case of (i) leads to the trivial solution where we have $M'=1$ and $\lambda=\omega$, while the second case (ii) is for the classical three-shock solution.

Now, we set $b\neq 0$, small and look for the solution ω' which is not far from its trivial solution, B can be simplified the case to B_0 with an approximation $\epsilon_2=0$ and $\lambda=\omega$ as

$$B_0 = B(\epsilon,\omega\,;\,0,\omega) = -\frac{2}{\gamma+1}\frac{\sqrt{M'^2-1}}{M'^2}+\frac{A'}{1+A'^2}\frac{1+\frac{2\gamma}{\gamma+1}}{\sin\omega\cos\omega} \times\left[-\frac{\gamma+1}{2}\frac{1+\epsilon}{\epsilon^2}A'+\frac{1}{2}\frac{\tan\omega}{1+\epsilon}\right] \tag{B4}$$

So that we have approximately,

$$\epsilon_2(\omega') = B_0^{-1}b' \tag{B5}$$

where ϵ_2 is given by (A1), (A2) and (A3) as

$$\epsilon_2' = M'^2\sin^2(\omega'+\delta')$$

and we have

$$M'^2\sin^2(\omega'+\delta') = 1+B_0^{-1}b'\,. \tag{B6}$$

We have also from the trivial solution ω_0', δ_0' ,

$$M'^2\sin^2(\omega_0'+\delta_0') = 1 \tag{B7}$$

(B6) and (B7) are combined to

$$M'^2B_0\sin(\omega'+\delta'+\omega_0'+\delta_0') \times\sin(\omega'+\delta'-\omega_0'-\delta_0') = b'\,. \tag{B8}$$

Since $\omega'+\delta'\approx\omega_0'+\delta_0'\approx 90°$ as we can see in Table 1 to a typical case, $sin(\omega'+\delta'+\omega_0'+\delta_0')\approx 0$ and accordingly magnitude of $\omega'+\delta'-\omega_0'-\delta_0'$ can be significant to a small b'. In fact, the magnitude of B_0 is of the order of one as we have $B_0=-0.43$, -0.44 to the typical cases of $M_i=1.2$, 1.4 ($\epsilon=0.44$, 0.98) with $\omega=60°$, and $b'=8.8\times10^{-4}$, 8.4×10^{-4} respectively for $M_i=1.2$, 1.4 when we assume $\omega'+\delta'+\omega_0'+\delta_0'=180°+1°, \omega'-\delta'-\omega_0'+\delta_0'=6°$.

References

Adachi T, Kobayashi S, Suzuki T (1992) Mach reflection of a weak plane shock wave. Proc. 11th Australasian Fluid Mech. Conf.: 279–282

Becker E (1961) Instanzionäre Grenzschichten hinter Verdichtungsstössen und Expansionswellen. Prog Aeronaut Sci 1, 104–73

Harrison FB, Bleakney, W (1947) Remeasurement of reflection angles in regular and Mach reflection of shock waves. Princeton Univ., Dept. Physics, Technical Report II-O

Henderson LF, Crutchfield WY, Virgona RJ (1997) The effects of thermal conductivity and viscosity of argon on shock waves diffracting over rigid ramps. J Fluid Mech 331, 1–36

Hornung H (1986) Regular and Mach reflection of shock waves. Ann Rev Fluid Mech 18, 33–58

Itabashi S, Henderson LF, Crutchfield WY, Takayama K (1997) Effects of viscous and thermal dissipation on the eruption of Mach reflection on rigid steel ramps. Proceedings of the 21st International Symposium on Shock Waves: 887–891

Kobayashi S, Adachi T, Satoh M, Suzuki T (1997) On the formation mechanism of the von Neumann reflection. Proceedings of the 21st International Symposium on Shock Waves: 881–885

Mirels H (1958) The wall boundary layer behind a moving shock wave. Grenzschichtforschung, Symposium Freiburg/Br., Springer-Verlag, pp. 283–292

Sakurai A (1964) On the problem of weak Mach reflection. Journal of the Physical Society of Japan 19, 1440–1450

Sakurai A, Henderson LF, Takayama K, Walenta Z, Collella P (1989) On the von Neumann paradox of weak Mach reflection. Fluid Dynamics Research 4, 333–345

Schlichting H (1979) Boundary-Layer Theory, 7th ed., McGraw-Hill, New York, pp. 439–443

Skews B (1999) Private communication at the 3rd Workshop on Shock Wave-Vortex Interaction

Walenta ZA (1987) Mach reflection of a moving, plane shock wave under rarefied flow conditions. Proceedings of the 16th International Symposium on Shock Waves: 535–541